

# Harmonic Wavelet Transform and Image Approximation

Zhijia Zhang and Naoki Saito

Dept. of Math., Univ. of California, Davis, California, 95616, USA.

Email: zhangzh@math.ucdavis.edu saito@math.ucdavis.edu

## Abstract

In 2006, Saito and Remy proposed a new transform called Laplace Local Sine Transform (LLST) in image processing as follows. Let  $f$  be a twice continuously differentiable function on a domain  $\Omega$ . First we approximate  $f$  by a harmonic function  $u$  such that the residual component  $v = f - u$  vanishes on the boundary of  $\Omega$ . Next, we do the odd extension for  $v$ , and then do the periodic extension, i.e. we obtain a periodic odd function  $v^*$ . Finally, we expand  $v^*$  into Fourier sine series. In this paper, we propose to expand  $v^*$  into a periodic wavelet series with respect to a biorthonormal periodic wavelet basis with the symmetric filter banks. We call this the *Harmonic Wavelet Transform* (HWT). HWT has an advantage over both LLST and the conventional wavelet transforms. On one hand, it removes the boundary mismatches as LLST does. On the other hand, the HWT coefficients reflect the local smoothness of  $f$  in the interior of  $\Omega$ . So the HWT algorithm approximates data more efficiently than LLST, periodic wavelet transform, folded wavelet transform, and wavelets on interval. We demonstrate the superiority of HWT over the other transforms using several standard images.

**Key words:** Harmonic wavelet transform, Laplace local sine transform, biorthonormal wavelets, periodic wavelets, folded wavelets, wavelets on interval, periodic wavelet coefficient, symmetry, odd extension.

## 1 Introduction

Wavelet analysis is an important tool in image processing. In order to approximate or compress data, there are two common wavelet algorithms: the periodic wavelet algorithm, and the folded wavelet algorithm. More precisely, let an image  $f$  be supported on a square  $\Omega \in \mathbb{R}^2$ . In the periodic wavelet algorithm, one extends  $f$  to a periodic function  $f^*$ , and then expands  $f^*$  into a periodic wavelet series using Daubechies wavelets [1] or polyharmonic spline wavelets [9]. Since  $f^*$  is discontinuous at the boundary points  $\partial\Omega$  in general, the decay rate of the corresponding periodic wavelet coefficients is very slow. Hence, in order to obtain a good approximation of the image, we need many periodic wavelet coefficients. In the folded wavelet algorithm, in order to avoid the boundary mismatches caused by the brute-force periodization, one does an even extension of  $f$ , and then extends it to a periodic function  $f^*$ , and finally expands  $f^*$  into a periodic wavelet series with respect to a biorthonormal periodic wavelet basis. If  $f$  is smooth, then  $f^* \in \text{lip}1$  on  $\mathbb{R}^2$ . This makes the decay rate of the

corresponding wavelet coefficients faster than that in periodic wavelets algorithm. But, since  $\frac{\partial}{\partial x} f^*$  and  $\frac{\partial}{\partial y} f^*$  are discontinuous at the boundary points, the decay rate of the periodic wavelet coefficients is still relatively low.

It is natural to ask how to ensure the continuity of derivatives of the periodized function across the boundary. In 2006, Saito and Remy [8] presented a good method: the Laplace Local Sine Transform (LLST) that ensures the derivatives of the periodized functions are continuous across the boundary. It decomposes an image  $f$  supported on a square  $\Omega$  into  $f = u + v$ , where  $u$  is a harmonic component satisfying Laplace's equation  $\Delta u = 0$  in  $\Omega$  and  $u = f$  on the boundary. After an odd extension, the residual component  $v$  is periodized to be  $v^*$ , i.e.,  $v^*$  is a periodic odd function. If  $f$  is smooth, then  $\frac{\partial}{\partial x} v^* \in \text{lip } 1$ ,  $\frac{\partial}{\partial y} v^* \in \text{lip } 1$  on  $\mathbb{R}^2$ . We call this method LLST decomposition. When one applies LLST to image approximation, one expands  $v^*$  into Fourier sine series.

In this paper, combining the LLST decomposition and the wavelet algorithm, we expand  $v^*$  into the periodic wavelet series. More precisely, we propose the harmonic wavelet transform (HWT). In the HWT algorithm, the first step is the same as LLST, i.e., we decompose  $f = u + v$  and obtain a periodic odd function  $v^*$ . Next, we choose a pair of real-valued biorthonormal wavelets  $\psi, \tilde{\psi}$  of  $L^2(\mathbb{R})$  generated by the real-valued even scaling functions  $\varphi, \tilde{\varphi}$ . Using a method of the tensor product and periodization, one gets a pair of biorthonormal periodic wavelet bases. Finally, we expand  $v^*$  into the periodic wavelet series with respect to this pair of biorthonormal periodic wavelet bases. Since  $\frac{\partial}{\partial x} v^* \in \text{lip } 1$  and  $\frac{\partial}{\partial y} v^* \in \text{lip } 1$  on  $\mathbb{R}^2$ , the decay rate of the corresponding periodic wavelet coefficients is faster than that of the periodic wavelet algorithm or the folded wavelet algorithm.

In general, the decay rate of the Fourier sine coefficients depends on global smoothness, while that of the periodic wavelet coefficients depends on local smoothness. Since the global smoothness of a function is determined by its rough part, we need fewer periodic wavelet coefficients than the Fourier sine coefficients in order to approximate the image with the same quality. Comparing the above several algorithms, the HWT

algorithm compresses data most efficiently among them.

In the HWT algorithm, we carefully study the symmetry of the periodic wavelet coefficients and show where these coefficients vanish. From this, we see that in order to recover the image exactly, the number of the efficient coefficients is just the same as the size of the sample points of  $f$ . So the HWT is not a redundant transform.

Our HWT algorithm is quite different from polyharmonic wavelets proposed by Van De Ville et al. [9], which are a kind of wavelet bases constructed by polyharmonic functions. The HWT has a different strategy: we approximate a target function by a harmonic function such that the residual part vanishes on the boundary, and then expand the residual part into wavelet series.

This paper is organized as follows. In Section 2, we recall the notions of biorthonormal periodic wavelet bases and the corresponding Mallat algorithm as well as the LLST algorithm. In Section 3, we present the HWT algorithm and show that in the one-dimensional case, the periodic wavelet algorithm, the folded wavelet algorithm, and the HWT algorithm generate periodic wavelet coefficients at the level  $m$  with the decay rates  $O(2^{-\frac{m}{2}})$ ,  $O(2^{-\frac{3m}{2}})$ , and  $O(2^{-\frac{5m}{2}})$ , respectively. When we use first  $2^M$  periodic wavelet coefficients, the obtained approximation error are  $o(1)$ ,  $O(2^{-M})$ , and  $O(2^{-2M})$ , respectively. In the two-dimensional case, the decay rates of the corresponding periodic wavelet coefficients are  $O(2^{-m})$ ,  $O(2^{-2m})$ , and  $O(2^{-3m})$ , respectively. When we use first  $2^{2M}$  periodic wavelet coefficients, the obtained approximation error are  $o(1)$ ,  $O(2^{-M})$ , and  $O(2^{-2M})$ , respectively. In Section 4, first, we discuss one-dimensional discrete HWT and the symmetry of the sequences consisting of the corresponding periodic wavelet coefficients. From this, we precisely show the efficient number of the periodic wavelet coefficients in order to recover a signal perfectly. Second, we discuss two-dimensional discrete HWT and the symmetry of the matrices of the corresponding periodic wavelet coefficients. From this, we precisely show the efficient number of the periodic wavelet coefficients in order to recover an image perfectly. In Section 5, we apply the HWT algorithm to approximate images and show that the HWT algorithm approximates images better than the LLST algorithm, the periodic wavelet algorithm, and the folded

wavelet algorithm.

## 2 Preliminaries

We state the well-known notions [4, 7] of biorthonormal periodic wavelet bases. After that, we recall the corresponding Mallat algorithms.

### 2.1 One-dimensional biorthonormal periodic wavelets

It is well-known that using the method of periodization, one can construct biorthonormal periodic wavelet bases with the help of the biorthonormal wavelets [4, 7].

Let  $\psi$  and  $\tilde{\psi}$  be a pair of compactly supported smooth biorthonormal wavelets of  $L^2(\mathbb{R})$  generated by compactly supported smooth scaling functions  $\varphi$  and  $\tilde{\varphi}$ . For  $m \in \mathbb{Z}$ ,  $n \in \mathbb{Z}$ , we denote the function family  $g_{m,n} := 2^{\frac{m}{2}} g(2^m \cdot -n)$ . Its periodization (with period 1) is  $g_{m,n}^{\text{per}} := \sum_{l \in \mathbb{Z}} g_{m,n}(\cdot + l)$ . The families

$$\Psi_1^{\text{per}} := \{\varphi^{\text{per}}\} \cup \{\psi_{m,n}^{\text{per}}, \quad m \in \mathbb{Z}_+, \quad n = 0, \dots, 2^m - 1\},$$

$$\tilde{\Psi}_1^{\text{per}} := \{\tilde{\varphi}^{\text{per}}\} \cup \{\tilde{\psi}_{m,n}^{\text{per}}, \quad m \in \mathbb{Z}_+, \quad n = 0, \dots, 2^m - 1\}$$

are called a pair of biorthonormal periodic wavelet bases for  $L^2\left(-\frac{1}{2}, \frac{1}{2}\right)$ .

Let  $f \in L^2\left(-\frac{1}{2}, \frac{1}{2}\right)$ . For  $m \in \mathbb{Z}_+$ ,  $n \in \mathbb{Z}$ , we denote the periodic wavelet coefficients

$$c_{m,n}^{(1)} := \int_{-\frac{1}{2}}^{\frac{1}{2}} f(t) \overline{\varphi_{m,n}^{\text{per}}(t)} dt, \quad d_{m,n}^{(1)} := \int_{-\frac{1}{2}}^{\frac{1}{2}} f(t) \overline{\tilde{\psi}_{m,n}^{\text{per}}(t)} dt. \quad (2.1)$$

Here the sequences  $\{c_{m,n}^{(1)}\}$  and  $\{d_{m,n}^{(1)}\}$  are periodic sequences (with period  $2^m$ ) with respect to the index  $n$ , i.e.,

$$c_{m,n+2^m l}^{(1)} = c_{m,n}^{(1)}, \quad d_{m,n+2^m l}^{(1)} = d_{m,n}^{(1)} \quad (l \in \mathbb{Z}).$$

It is well known that

$$f = c_{0,0}^{(1)} + \sum_{m=0}^{\infty} \sum_{n=0}^{2^m-1} d_{m,n}^{(1)} \tilde{\psi}_{m,n}^{\text{per}} \quad (2.2)$$

in the space  $L^2([-\frac{1}{2}, \frac{1}{2}])$ . For  $M \in \mathbb{Z}_+$ , its  $2^M$ -partial sum is

$$S_{2^M}(f) = c_{0,0}^{(1)} + \sum_{m=0}^{M-1} \sum_{n=0}^{2^m-1} d_{m,n}^{(1)} \tilde{\psi}_{m,n}^{\text{per}}. \quad (2.3)$$

Let the space  $\tilde{V}_m$  be the span of  $\{\tilde{\varphi}_{m,n}^{\text{per}}\}_{n=0,\dots,2^m-1}$ . One can decompose the projection of  $f$  in  $\tilde{V}_m$  as follows [7].

$$P_{\tilde{V}_m}(f) = \sum_{n=0}^{2^m-1} c_{m,n}^{(1)} \tilde{\varphi}_{m,n}^{\text{per}} = \sum_{n=0}^{2^{m-1}-1} c_{m-1,n}^{(1)} \tilde{\varphi}_{m-1,n}^{\text{per}} + \sum_{n=0}^{2^{m-1}-1} d_{m-1,n}^{(1)} \tilde{\psi}_{m-1,n}^{\text{per}}. \quad (2.4)$$

Now we assume that  $\varphi$  and  $\tilde{\varphi}$  are both compactly supported. Denote the coefficients of the filter banks

$$a_k := \sqrt{2} \int_{\mathbb{R}} \varphi(t) \overline{\tilde{\varphi}(2t-k)} dt, \quad b_k := \sqrt{2} \int_{\mathbb{R}} \psi(t) \overline{\tilde{\varphi}(2t-k)} dt. \quad (2.5)$$

Without loss of generality, we assume that for some  $N \in \mathbb{Z}_+$ ,

$$a_n = b_{n+1} = 0 \quad (|n| \geq N). \quad (2.6)$$

Mallat showed that the fast algorithm to compute periodic wavelet coefficients is similar to the fast algorithm of wavelet coefficients [7, Sec. 7.5.1]. Along Mallat's idea, one can obtain the following algorithm for the one-dimensional periodic wavelet coefficients.

**Proposition 2.1.** Let the filters  $a_k, b_k$  be defined in (2.5) and  $c_{m,n}^{(1)}, d_{m,n}^{(1)}$  be defined in (2.3). Define

$$a_n^* := a_n, \quad b_{n+1}^* := b_{n+1} \quad (|n| \leq 2^{J-1}), \quad a_{n+2^J}^* := a_n^*, \quad b_{n+2^J}^* := b_n^* \quad (n \in \mathbb{Z}). \quad (2.7)$$

Then for  $2^{J-1} \geq N$ , we have

$$c_{J-1,k}^{(1)} = \sum_{n=0}^{2^J-1} \overline{a_{n-2k}^*} c_{J,n}^{(1)}, \quad d_{J-1,k}^{(1)} = \sum_{n=0}^{2^J-1} \overline{b_{n-2k}^*} c_{J,n}^{(1)}, \quad k \in \mathbb{Z} \quad (2.8)$$

## 2.2 Two-dimensional biorthonormal periodic wavelets

Let  $\psi$  and  $\tilde{\psi}$  be a pair of biorthonormal wavelets generated by the scaling functions  $\varphi$  and  $\tilde{\varphi}$ . Take the tensor products of  $\varphi, \psi$ . Denote

$$\varphi_0(x, y) := \varphi(x)\varphi(y), \quad \psi_1(x, y) := \varphi(x)\psi(y),$$

$$\psi_2(x, y) := \psi(x)\varphi(y), \quad \psi_3(x, y) := \psi(x)\psi(y).$$

Similarly, taking the tensor products of  $\tilde{\varphi}$  and  $\tilde{\psi}$ , we get  $\tilde{\varphi}_0(x, y)$ ,  $\tilde{\psi}_1(x, y)$ ,  $\tilde{\psi}_2(x, y)$ , and  $\tilde{\psi}_3(x, y)$ . Then  $\{\psi_\mu\}_1^3$  and  $\{\tilde{\psi}_\mu\}_1^3$  are a pair of biorthonormal wavelets generated by the scaling functions  $\varphi_0$  and  $\tilde{\varphi}_0$ , respectively.

The families

$$\Psi_2^{\text{per}} = \{\varphi_0^{\text{per}}\} \cup \{\psi_{\mu,m,n}^{\text{per}}, \quad \mu = 1, 2, 3, \quad m \in \mathbb{Z}_+, \quad n = (n_1, n_2), \quad n_1, n_2 = 0, \dots, 2^m - 1\},$$

$$\tilde{\Psi}_2^{\text{per}} = \{\tilde{\varphi}_0^{\text{per}}\} \cup \{\tilde{\psi}_{\mu,m,n}^{\text{per}}, \quad \mu = 1, 2, 3, \quad m \in \mathbb{Z}_+, \quad n = (n_1, n_2), \quad n_1, n_2 = 0, \dots, 2^m - 1\}.$$

are called a pair of biorthonormal periodic wavelet bases for  $L^2\left(\left[-\frac{1}{2}, \frac{1}{2}\right]^2\right)$ .

Let  $f \in L^2\left(\left[-\frac{1}{2}, \frac{1}{2}\right]^2\right)$ . For  $\mu = 1, 2, 3$ ,  $m \in \mathbb{Z}_+$ ,  $n \in \mathbb{Z}^2$ , we denote the periodic wavelet coefficients

$$c_{m,n}^{(2)} := \int_{\frac{1}{2}}^{\frac{1}{2}} \int_{-\frac{1}{2}}^{\frac{1}{2}} f(x, y) \overline{\varphi_{0,m,n}^{\text{per}}(x, y)} dx dy, \quad d_{\mu,m,n}^{(2)} := \int_{-\frac{1}{2}}^{\frac{1}{2}} \int_{-\frac{1}{2}}^{\frac{1}{2}} f(x, y) \overline{\psi_{\mu,m,n}^{\text{per}}(x, y)} dx dy. \quad (2.9)$$

Here the sequences  $\{c_{m,n}^{(2)}\}$  and  $\{d_{\mu,m,n}^{(2)}\}$  are periodic sequences with respect to  $n$ , i.e.

$$c_{m,n+2^m l}^{(2)} = c_{m,n}^{(2)}, \quad d_{\mu,m,n+2^m l}^{(2)} = d_{\mu,m,n}^{(2)} \quad (l \in \mathbb{Z}^2).$$

It is well known that

$$f = c_{0,0}^{(2)} + \sum_{\mu=1}^3 \sum_{m=0}^{\infty} \sum_{n_1, n_2=0}^{2^m-1} d_{\mu,m,n}^{(2)} \tilde{\psi}_{\mu,m,n}^{\text{per}}. \quad (2.10)$$

For  $M \in \mathbb{Z}_+$ , its  $2^{2M}$ -partial sum is

$$S_{2^{2M}}(f) = c_{0,0}^{(2)} + \sum_{\mu=1}^3 \sum_{m=0}^{M-1} \sum_{n_1, n_2=0}^{2^m-1} d_{\mu,m,n}^{(2)} \tilde{\psi}_{\mu,m,n}^{\text{per}}$$

in the space  $L^2\left(\left[-\frac{1}{2}, \frac{1}{2}\right]^2\right)$ , where  $n = (n_1, n_2)$ .

Let the space  $\tilde{V}_m$  be the span of  $\{\tilde{\varphi}_{0,m,n}^{\text{per}}\}_{n=(n_1, n_2), n_1, n_2=0, \dots, 2^m-1}$ . One can decompose the project of  $f$  in  $\tilde{V}_m$  as follows.

$$P_{\tilde{V}_m}(f) = \sum_{n_1, n_2=0}^{2^m-1} c_{m,n}^{(2)} \tilde{\varphi}_{0,m,n}^{\text{per}} = \sum_{n_1, n_2=0}^{2^{m-1}-1} c_{m-1,n}^{(2)} \tilde{\varphi}_{0,m-1,n}^{\text{per}} + \sum_{\mu=1}^3 \sum_{n_1, n_2=0}^{2^{m-1}-1} d_{\mu,m-1,n}^{(2)} \tilde{\psi}_{\mu,m-1,n}^{\text{per}}. \quad (2.11)$$

From the Mallat algorithm of the one-dimensional periodic wavelet, one can easily conclude the following Mallat algorithm for two-dimensional tensor product periodic wavelets.

**Proposition 2.2.** Let the filters  $\{a_n^*\}, \{b_n^*\}$  be stated in (2.7) and the periodic wavelet coefficients  $c_{m,n}^{(2)}, d_{\mu,m,n}^{(2)}$  be stated in (2.9). Then for  $J > N$  and  $k = (k_1, k_2) \in \mathbb{Z}^2$ , we have

$$\begin{aligned}
\text{(i)} \quad c_{J-1,k}^{(2)} &= \sum_{n_1, n_2=0}^{2^J-1} \overline{a_{n_1-2k_1}^*} \overline{a_{n_2-2k_2}^*} c_{J,n_1,n_2}^{(2)}, \\
\text{(ii)} \quad d_{1,J-1,k}^{(2)} &= \sum_{n_1, n_2=0}^{2^J-1} \overline{a_{n_1-2k_1}^*} \overline{b_{n_2-2k_2}^*} c_{J,n_1,n_2}^{(2)}, \\
\text{(iii)} \quad d_{2,J-1,k}^{(2)} &= \sum_{n_1, n_2=0}^{2^J-1} \overline{b_{n_1-2k_1}^*} \overline{a_{n_2-2k_2}^*} c_{J,n_1,n_2}^{(2)}, \\
\text{(iv)} \quad d_{3,J-1,k}^{(2)} &= \sum_{n_1, n_2=0}^{2^J-1} \overline{b_{n_1-2k_1}^*} \overline{b_{n_2-2k_2}^*} c_{J,n_1,n_2}^{(2)}.
\end{aligned}$$

### 2.3 Laplace local sine transforms

First we consider the one-dimensional case. Let  $\Omega_1 := [0, \frac{1}{2}]$  and the function  $f$  be defined on  $\Omega_1$  and  $f \in C^2(\Omega_1)$ .

We split the function  $f$  into two components

$$f(x) = u(x) + v(x) \quad \text{on } \Omega_1.$$

The first function  $u(x) = 2(f(\frac{1}{2}) - f(0))x + f(0)$  and the second function satisfies

$$v(0) = v\left(\frac{1}{2}\right) = 0.$$

After an odd extension, the second function  $v$  is periodized to be  $v^*$ , i.e.,  $v^*$  is a periodic odd function. Finally we expand  $v^*$  into Fourier sine series.

Next, we consider the two-dimensional case. Let  $\Omega_2 := [0, \frac{1}{2}]^2$  and the function  $f$  be defined on  $\Omega_2$  and  $f \in C^2(\Omega_2)$ . We split the function  $f$  into two components

$$f(x, y) = u(x, y) + v(x, y) \quad \text{on } \Omega_2.$$

where  $u(x, y)$  is the harmonic function which satisfies Laplace's equation  $\Delta u(x, y) = 0$  ( $(x, y) \in \Omega_2$ ) and  $u(x, y) = f(x, y)$  on the boundary of  $\Omega_2$ . So the residual satisfies

$$v(x, y) = 0 \quad ((x, y) \in \partial\Omega_2).$$

After an odd extension, the residual component  $v$  is periodized to be  $v^*$ , i.e.,  $v^*$  is a periodic odd function. Finally we expand  $v^*$  into Fourier sine series.

### 3 Harmonic Wavelet Transform

Now we present a notion of the *Harmonic Wavelet Transform* (HWT). We show that for the HWT algorithm, the decay rate of periodic wavelet coefficients is the faster than those generated by the periodic wavelet transform algorithm and the folded wavelet algorithm.

#### 3.1 One-dimensional HWT algorithm

We assume that  $f$  is defined on  $[0, \frac{1}{2}]$ . Let

$$f(t) = u(t) + v(t) \quad \left( t \in \left[0, \frac{1}{2}\right] \right),$$

where  $u(t) = 2(f(\frac{1}{2}) - f(0))t + f(0)$  and the residual component  $v(t)$  satisfies  $v(0) = v(\frac{1}{2}) = 0$ .

We do the odd extension  $v_{\text{odd}}$  of the residual component  $v$  to  $[-\frac{1}{2}, \frac{1}{2}]$ . We again do the 1-periodic extension of  $v_{\text{odd}}$ , denoted by  $v^*$ . Finally, we expand  $v^*$  into the biorthonormal periodic wavelet series. We call this process the one-dimensional HWT.

Now we examine the decay rates of the coefficients of various wavelet algorithms in the one-dimensional case.

(i) The 1D periodic wavelet algorithm. Let  $f \in C^2([-\frac{1}{2}, \frac{1}{2}])$ . In the periodic wavelet algorithm, we directly expand  $f$  into biorthonormal periodic wavelet series. Clearly, the coefficients

$$d_{m,n}^{(1)} = \int_{-\frac{1}{2}}^{\frac{1}{2}} f(t) \overline{\psi_{m,n}^{\text{per}}(t)} dt = \int_{\mathbb{R}} f^*(t) \overline{\psi_{m,n}(t)} dt = 2^{\frac{m}{2}} \int_{\mathbb{R}} f^*(t) \overline{\psi(2^m t - n)} dt, \quad (3.1)$$

where  $f^*$  is the 1-periodic extension of  $f$ . Since  $f^* \in L^\infty(\mathbb{R})$ ,  $\psi \in L^1(\mathbb{R})$ , we have

$$d_{m,n}^{(1)} = O(2^{\frac{m}{2}}) \int_{\mathbb{R}} |\psi(2^m t - n)| dt = O(2^{-\frac{m}{2}}) \int_{\mathbb{R}} |\psi(t - n)| dt = O(2^{-\frac{m}{2}}) \int_{\mathbb{R}} |\psi(t)| dt = O(2^{-\frac{m}{2}}). \quad (3.2)$$

(ii) The 1D folded wavelet algorithm. Let  $f \in C^2\left([0, \frac{1}{2}]\right)$ . In the folded wavelet algorithm, we do an even extension of  $f$

$$f_{\text{even}}(x) = \begin{cases} f(t), & t \in [0, \frac{1}{2}], \\ f(-t), & t \in [-\frac{1}{2}, 0]. \end{cases}$$

Then

$$f_{\text{even}}(x) \in C\left[-\frac{1}{2}, \frac{1}{2}\right] \quad \text{and} \quad f_{\text{even}}\left(-\frac{1}{2}\right) = f_{\text{even}}\left(\frac{1}{2}\right),$$

Again let  $f^*(t)$  be a 1-periodic extension of  $f_{\text{even}}(t)$ , we have

**Proposition 3.1.** The periodic wavelet coefficients of  $f^*$  satisfy

$$d_{m,n}^{(1)} = O\left(2^{-\frac{3m}{2}}\right). \quad (3.3)$$

The partial sum  $S_{2^M}(f^*)$  of the periodic wavelet expansion of  $f^*$  satisfies

$$\|f^* - S_{2^M}(f^*)\|_{L^2\left([-\frac{1}{2}, \frac{1}{2}]\right)} = O\left(2^{-M}\right). \quad (3.4)$$

**Proof.** Since  $f \in C^2\left[0, \frac{1}{2}\right]$ , we have  $f^* \in \text{lip } 1$  on  $\mathbb{R}$ , i.e., there is a constant  $K$  such that

$$\left|f^*(t) - f^*\left(\frac{n}{2^m}\right)\right| \leq K \left|t - \frac{n}{2^m}\right| \quad (t \in \mathbb{R}).$$

Since  $f^* \in \text{lip } 1$ ,  $\int_{\mathbb{R}} \psi(t) dt = 0$ , and (3.1), we have

$$\begin{aligned} \left|d_{m,n}^{(1)}\right| &= \left|2^{\frac{m}{2}} \int_{\mathbb{R}} f^*(t) \overline{\psi(2^m t - n)} dt\right| = \left|2^{\frac{m}{2}} \int_{\mathbb{R}} \left(f^*(t) - f^*\left(\frac{n}{2^m}\right)\right) \overline{\psi(2^m t - n)} dt\right| \\ &\leq K 2^{\frac{m}{2}} \int_{\mathbb{R}} \left|t - \frac{n}{2^m}\right| |\psi(2^m t - n)| dt = K 2^{-\frac{3m}{2}} \int_{\mathbb{R}} |t - n| |\psi(t - n)| dt \\ &= K 2^{-\frac{3m}{2}} \int_{\mathbb{R}} |t\psi(t)| dt = O\left(2^{-\frac{3m}{2}}\right). \end{aligned}$$

So (3.3) holds.

By (2.2) and (2.3), we know that the difference between  $f^*$  and the partial sum of its periodic wavelet series

$$f^* - S_{2^{M+1}}(f^*) = \sum_{m=M}^{\infty} \sum_{n=0}^{2^m-1} d_{m,n}^{(1)} \overline{\widetilde{\psi}_{m,n}^{\text{per}}}$$

is in the space  $L^2\left(-\frac{1}{2}, \frac{1}{2}\right)$ . Using the Parseval equality and (3.3), we get

$$\begin{aligned} \|f^* - S_{2^M}(f^*)\|_{L^2\left(-\frac{1}{2}, \frac{1}{2}\right)}^2 &= \sum_{m=M}^{\infty} \sum_{n=0}^{2^m-1} |d_{m,n}^{(1)}|^2 = O(1) \sum_{m=M}^{\infty} \sum_{n=0}^{2^m-1} \left(2^{-\frac{3m}{2}}\right)^2 \\ &= O(1) \sum_{m=M}^{\infty} 2^{-2m} = O(2^{-2M}). \end{aligned}$$

So (3.4) holds. Proposition 3.1 is proved.  $\square$

(iii) The 1D HWT algorithm. Let  $f \in C^2\left([0, \frac{1}{2}]\right)$ . Now we introduce the HWT algorithm.

(a) We first decompose  $f$  on  $[0, \frac{1}{2}]$  as follows

$$f(x) = u(x) + v(x) \quad \left(x \in \left[0, \frac{1}{2}\right]\right),$$

where  $u(x) = 2\left(f\left(\frac{1}{2}\right) - f(0)\right)x + f(0)$ . So  $v(0) = v\left(\frac{1}{2}\right) = 0$ .

(b) We do the odd extension of  $v$ , i.e., let

$$v_{\text{odd}}(t) = v(t) \quad \left(t \in \left[0, \frac{1}{2}\right]\right) \quad \text{and} \quad v_{\text{odd}}(-t) = -v(t) \quad \left(t \in \left[0, \frac{1}{2}\right]\right).$$

So  $v_{\text{odd}}\left(\frac{1}{2}\right) = v_{\text{odd}}\left(-\frac{1}{2}\right) = v_{\text{odd}}(0) = 0$ . Since  $\frac{v_{\text{odd}}(-x)}{-x} = \frac{v_{\text{odd}}(x)}{x}$ , letting  $x \rightarrow 0^+$ , we get  $(v_{\text{odd}})'_{-}(0) = (v_{\text{odd}})'_{+}(0)$ . Hence  $v_{\text{odd}}(t)$  is differentiable at  $t = 0$ .

(c) We do the 1-periodic extension  $v^*$  of  $v_{\text{odd}}$ , i.e.,  $v^*$  is a 1-periodic function and  $v^*(t) = v_{\text{odd}}(t)$  ( $|t| \leq \frac{1}{2}$ ).

Furthermore, we easily prove  $\frac{d}{dt}v^* \in \text{lip } 1$  on  $\mathbb{R}$ .

**Proposition 3.2.** Let  $v^*$  be stated as above, i.e.,  $v^*$  is a 1-periodic function and  $\frac{dv^*}{dt} \in \text{lip } 1$  on  $\mathbb{R}$ . Then the periodic wavelet coefficients of  $v^*$  satisfy

$$d_{m,n}^{(1)} = O\left(2^{-\frac{5m}{2}}\right). \quad (3.5)$$

The partial sum  $S_{2^{M+1}}(v^*)$  of the periodic wavelet expansion of  $v^*$  satisfies

$$\|v^* - S_{2^{M+1}}(v^*)\|_{L^2\left(-\frac{1}{2}, \frac{1}{2}\right)} = O(2^{-2M}). \quad (3.6)$$

**Proof.** Since  $\int_{\mathbb{R}} \psi(t) dt = 0$  and  $\int_{\mathbb{R}} t\psi(t) dt = 0$ , we have

$$d_{m,n}^{(1)} = 2^{\frac{m}{2}} \int_{\mathbb{R}} v^*(t) \overline{\psi(2^m t - n)} dt = 2^{\frac{m}{2}} \int_{\mathbb{R}} \left(v^*(t) - v^*\left(\frac{n}{2^m}\right) - v^{*'}\left(\frac{n}{2^m}\right)\left(t - \frac{n}{2^m}\right)\right) \overline{\psi(2^m t - n)} dt. \quad (3.7)$$

Again, since  $\frac{dv^*}{dt} \in \text{lip } 1$  on  $\mathbb{R}$ , we know that there is a constant  $K$  such that for any  $t_0 \in \mathbb{R}$ ,

$$|v^{*'}(t) - v^{*'}(t_0)| \leq K|t - t_0| \quad (t \in \mathbb{R}).$$

This implies that

$$|v^*(t) - v^*(t_0) - v^{*'}(t_0)(t - t_0)| = \left| \int_{t_0}^t (v^{*'}(t) - v^{*'}(t_0)) dt \right| \leq K(t - t_0)^2 \quad (t \in \mathbb{R}).$$

Taking  $t_0 = \frac{n}{2^m}$  in this formula, by (3.7) we have

$$\left| d_{m,n}^{(1)} \right| \leq K 2^{\frac{m}{2}} \int_{\mathbb{R}} \left( t - \frac{n}{2^m} \right)^2 |\psi(2^m t - n)| dt = K 2^{-\frac{5m}{2}} \int_{\mathbb{R}} t^2 |\psi(t)| dt = O\left(2^{-\frac{5m}{2}}\right). \quad (3.8)$$

By the similar argument to (3.4), from (3.8) we now have

$$\|v^* - S_{2^M}(v^*)\|_{L^2([- \frac{1}{2}, \frac{1}{2}])} = O(2^{-2M}).$$

So (3.6) holds. Proposition 3.2 is proved.  $\square$

### 3.2 Two-dimensional HWT algorithm

We assume that  $f$  is defined on  $[0, \frac{1}{2}]^2$ . Let

$$f(x, y) = u(x, y) + v(x, y) \quad \left( (x, y) \in \left[0, \frac{1}{2}\right]^2 \right),$$

where  $u(x, y)$  is a harmonic function and  $v(x, y)$  satisfies  $v(x, y) = 0$  for  $(x, y) \in \partial\left([0, \frac{1}{2}]^2\right)$ . We do the odd extension  $v_{\text{odd}}$  of the residual component  $v$  to  $[-\frac{1}{2}, \frac{1}{2}]^2$ , that is,

$$v_{\text{odd}}(x, y) = v(x, y) \quad \left( (x, y) \in \left[0, \frac{1}{2}\right]^2 \right)$$

and

$$v_{\text{odd}}(-x, y) = v_{\text{odd}}(x, -y) = -v_{\text{odd}}(x, y) \quad \left( (x, y) \in \left[-\frac{1}{2}, \frac{1}{2}\right]^2 \right).$$

Again we do the 1-periodic extension of  $v_{\text{odd}}$ , denoted by  $v^*$ . Finally, we expand  $v^*$  into a biorthonormal periodic wavelet series. We call this process the two-dimensional HWT.

Now we examine the decay rates of the coefficients of various wavelet algorithms in the two-dimensional case.

(i) The 2D periodic wavelet algorithm. Let  $f \in C^2\left(\left[-\frac{1}{2}, \frac{1}{2}\right]^2\right)$ . Denote the 1-periodic extension of  $f$  on  $\mathbb{R}^2$  by  $f^*$ . By (2.9), the periodic wavelet coefficients are

$$d_{\mu,m,n}^{(2)} = \int_{\mathbb{R}} \int_{\mathbb{R}} f^*(x, y) \overline{\psi_{\mu,m,n}(x, y)} dx dy \quad (\mu = 1, 2, 3).$$

So, for each  $\mu$ , we have

$$\begin{aligned} |d_{\mu,m,n}^{(2)}| &= \left| 2^m \int_{\mathbb{R}} \int_{\mathbb{R}} f^*(x, y) \overline{\psi_{\mu}(2^m x - n_1, 2^m y - n_2)} dx dy \right| \\ &= O(2^{-m}) \int_{\mathbb{R}} \int_{\mathbb{R}} |\psi_{\mu}(x - n_1, y - n_2)| dx dy \\ &= O(2^{-m}) \int_{\mathbb{R}} \int_{\mathbb{R}} |\psi_{\mu}(x, y)| dx dy = O(2^{-m}). \end{aligned}$$

(ii) The 2D folded wavelet algorithm. Let  $f \in C^2\left(\left[0, \frac{1}{2}\right]^2\right)$ , we do an even extension to  $\left[-\frac{1}{2}, \frac{1}{2}\right]^2$ , and then we do a 1-periodic extension to  $\mathbb{R}^2$ , denoted by  $f_2$ . Then  $f_2 \in \text{lip } 1$  on  $\mathbb{R}^2$ .

**Proposition 3.3.** Let  $f_2$  be stated as above, i.e.,  $f_2$  is a 1-periodic function and  $f_2 \in \text{lip } 1$  on  $\mathbb{R}^2$ . Then the periodic wavelet coefficients of  $f_2$  satisfy

$$d_{\mu,m,n}^{(2)} = O(2^{-2m}). \quad (3.9)$$

The partial sum  $S_{2^{2M}}$  of the periodic wavelet expansion of  $f_2$  satisfies

$$\|f_2 - S_{2^{2M}}(f_2)\|_{L^2\left(\left[-\frac{1}{2}, \frac{1}{2}\right]^2\right)} = O(2^{-M}). \quad (3.10)$$

**Proof.** Let  $z = (x, y)$ . Since  $f_2 \in \text{lip } 1(\mathbb{R}^2)$  and  $\int_{\mathbb{R}} \psi(z) dz = 0$ , we have

$$d_{\mu,m,n}^{(2)} = \int_{\mathbb{R}^2} f_2(z) \overline{\psi_{\mu,m,n}(z)} dz = \int_{\mathbb{R}^2} \left(f_2(z) - f_2\left(\frac{n}{2^m}\right)\right) \overline{\psi_{\mu,m,n}(z)} dz,$$

so

$$|d_{\mu,m,n}^{(2)}| = O(2^m) \int_{\mathbb{R}^2} \left|z - \frac{n}{2^m}\right| |\psi_{\mu}(2^m z - n)| dz = O(2^{-2m}) \int_{\mathbb{R}^2} \int_{\mathbb{R}^2} |\psi_{\mu}(z)| dz = O(2^{-2m}).$$

So (3.9) holds.

By (2.10), we know that the difference between  $f_2$  and the partial sum of its periodic wavelet series

$$f_2 - S_{2^{2M}}(f_2) = \sum_{\mu=1}^3 \sum_{m=M}^{\infty} \sum_{n=0}^{2^m-1} d_{\mu,m,n}^{(2)} \overline{\widetilde{\psi}_{\mu,m,n}^{\text{per}}}$$

is in the space  $L^2\left([-\frac{1}{2}, \frac{1}{2}]^2\right)$ . Using the Parseval equality, we have

$$\|f_2 - S_{2^{2M}}(f_2)\|_{L^2\left([-\frac{1}{2}, \frac{1}{2}]^2\right)}^2 = \sum_{\mu=1}^3 \sum_{m=M}^{\infty} \sum_{n_1=0}^{2^m-1} \sum_{n_2=0}^{2^m-1} \left|d_{\mu,m,n}^{(2)}\right|^2,$$

where  $n = (n_1, n_2) \in \mathbb{Z}_+^2$ . Again, by  $d_{\mu,m,n}^{(2)} = O(2^{-2m})$ , we have

$$\|f_2 - S_{2^{2M}}(f_2)\|_{L^2\left([-\frac{1}{2}, \frac{1}{2}]^2\right)}^2 = O(1) \sum_{m=M}^{\infty} 2^{-2m} = O(2^{-2M}).$$

So we get (3.10). Proposition 3.3 is proved.  $\square$

(iii) The 2D HWT algorithm. We can easily prove that 1-periodic function  $v^*$  satisfies

$$\frac{\partial v^*}{\partial x}(x, y) \in \text{lip } 1 \quad \text{and} \quad \frac{\partial v^*}{\partial y}(x, y) \in \text{lip } 1 \quad ((x, y) \in \mathbb{R}^2). \quad (3.11)$$

**Proposition 3.4.** Let  $v^*$  be stated as above, i.e.,  $v^*$  is a 1-periodic function and (3.11) holds. Then the periodic wavelet coefficients of  $v^*$  satisfy

$$d_{\mu,m,n}^{(2)} = O(2^{-3m}). \quad (3.12)$$

The partial sum  $S_{2^{2M}}(v^*)$  of the periodic wavelet expansion of  $v^*$  satisfies

$$\|v^* - S_{2^{2M}}(v^*)\|_{L^2\left([-\frac{1}{2}, \frac{1}{2}]^2\right)} = O(2^{-2M}). \quad (3.13)$$

**Proof.** For  $z = (x, y)$  and  $z_0 = (x_0, y_0)$ , we have

$$\begin{aligned}
v^*(z) - v^*(z_0) - \frac{\partial v^*}{\partial x}(z_0)(x - x_0) - \frac{\partial v^*}{\partial y}(z_0)(y - y_0) &= \int_{x_0}^x \left( \frac{\partial v^*}{\partial x}(x, y_0) - \frac{\partial v^*}{\partial x}(x_0, y_0) \right) dx \\
&+ \int_{y_0}^y \left( \frac{\partial v^*}{\partial y}(x, y) - \frac{\partial v^*}{\partial y}(x, y_0) \right) dy \\
&+ \int_{y_0}^y \left( \frac{\partial v^*}{\partial y}(x, y_0) - \frac{\partial v^*}{\partial y}(x_0, y_0) \right) dy \\
&=: J_1 + J_2 + J_3.
\end{aligned} \tag{3.14}$$

By (3.11), we get

$$\begin{aligned}
|J_1| &\leq K(x - x_0)^2 \leq K|z - z_0|^2, \\
|J_2| &\leq K(y - y_0)^2 \leq K|z - z_0|^2, \\
|J_3| &\leq K|x - x_0| |y - y_0| \leq \frac{K}{2} ((x - x_0)^2 + (y - y_0)^2) = \frac{K}{2}|z - z_0|^2.
\end{aligned}$$

Again, by (3.14),

$$\left| v^*(z) - v^*(z_0) - \frac{\partial v^*}{\partial x}(z_0)(x - x_0) - \frac{\partial v^*}{\partial y}(z_0)(y - y_0) \right| \leq 3K|z - z_0|^2. \tag{3.15}$$

By the definition of  $\psi_\mu(x, y)$  ( $\mu = 1, 2, 3$ ), we obtain that for  $\mu = 1, 2, 3$ ,

$$\int_{\mathbb{R}^2} x\psi_\mu(z) dz = \int_{\mathbb{R}^2} y\psi_\mu(z) dz = \int_{\mathbb{R}^2} \psi_\mu(z) dz = 0. \tag{3.16}$$

By (2.9) and (3.16), taking  $z_0 = (x_0, y_0) = \frac{n}{2^m}$  ( $n = (n_1, n_2)$ ), we deduce that

$$\begin{aligned}
d_{\mu, m, n}^{(2)} &= 2^m \int_{\mathbb{R}^2} v^*(z) \overline{\psi_\mu(2^m z - n)} dz \\
&= 2^m \int_{\mathbb{R}^2} \left( v^*(z) - v^*\left(\frac{n}{2^m}\right) - \frac{\partial v^*}{\partial x}\left(\frac{n}{2^m}\right)\left(x - \frac{n_1}{2^m}\right) - \frac{\partial v^*}{\partial y}\left(\frac{n}{2^m}\right)\left(y - \frac{n_2}{2^m}\right) \right) \overline{\psi_\mu(2^m z - n)} dz.
\end{aligned}$$

From this and (3.15), noticing that  $x_0 = \frac{n_1}{2^m}$  and  $y_0 = \frac{n_2}{2^m}$ , we have

$$\left| d_{\mu, m, n}^{(2)} \right| \leq 3K 2^m \int_{\mathbb{R}^2} \left| z - \frac{n}{2^m} \right|^2 |\psi_\mu(2^m z - n)| dz \leq 3K 2^{-3m} \int_{\mathbb{R}^2} |z|^2 |\psi_\mu(z)| dz = O(2^{-3m}). \tag{3.17}$$

So (3.12) holds.

By the similar argument to (3.10) above, from (3.7) we now have

$$\|v^* - S_{2^{2M}}(v^*)\|_{L^2\left([-\frac{1}{2}, \frac{1}{2}]^2\right)} = O(2^{-2M}).$$

Proposition 3.4 is proved.  $\square$

## 4 Discrete HWT

In this section, we will discuss the discrete HWT and study the symmetry property of the coefficients.

We always assume that  $\psi$  and  $\tilde{\psi}$  be a pair of biorthonormal wavelets generated by the scaling functions  $\varphi$ ,  $\tilde{\varphi}$  that are compactly supported real-valued even functions. We also assume that  $\psi$  and  $\tilde{\psi}$  are real-valued functions. Let the filters  $\{a_k\}$  and  $\{b_k\}$  be defined in (2.5) and let us assume the formula (2.6) holds. Since  $\varphi$  and  $\tilde{\varphi}$  are symmetric at  $t = 0$ , by the known result [4], we know that  $\psi$  and  $\tilde{\psi}$  are symmetric at  $t = \frac{1}{2}$  and  $t = -\frac{1}{2}$ , respectively.

### 4.1 Definition of one-dimensional discrete HWT

Let  $f \in C^2\left([0, \frac{1}{2}]\right)$  be a signal of the interval  $[0, \frac{1}{2}]$ . We are given the discretized version of  $f$  sampled at  $\left\{\frac{n}{2^J}\right\}_{n=0}^{2^J-1}$ :

$$x_n = f\left(\frac{n}{2^J}\right) \quad (n = 0, \dots, 2^J-1).$$

Then  $x_0 = f(0)$  and  $x_{2^J-1} = f(\frac{1}{2})$ . Using the HWT decomposition, we get

$$f(t) = 2 \left( f\left(\frac{1}{2}\right) - f(0) \right) t + f(0) + v(t) = 2(x_{2^J-1} - x_0)t + x_0 + v(t) \quad \left(0 \leq t \leq \frac{1}{2}\right).$$

So, for  $n = 0, \dots, 2^J-1$ ,

$$y_n := v\left(\frac{n}{2^J}\right) = x_n - (x_{2^J-1} - x_0)\frac{n}{2^J-1} - x_0.$$

In particular,  $y_0 = y_{2^J-1} = 0$ .

Since the odd extension  $v_{\text{odd}}$  of  $v$  to  $[-\frac{1}{2}, \frac{1}{2}]$  satisfies

$$v_{\text{odd}}(t) = -v(-t) \quad \left( t \in \left[ -\frac{1}{2}, 0 \right] \right),$$

the sequence  $\{y_n^{\text{odd}}\}_{n=-2^{J-1}}^{2^{J-1}}$ , where  $y_n^{\text{odd}} := v_{\text{odd}}\left(\frac{n}{2^J}\right)$ , satisfies the conditions

$$y_n^{\text{odd}} = -y_{-n}^{\text{odd}} \quad (-2^{J-1} \leq n \leq 2^{J-1}) \quad \text{and} \quad y_0^{\text{odd}} = y_{2^{J-1}}^{\text{odd}} = y_{-2^{J-1}}^{\text{odd}} = 0.$$

Let  $v^*$  be a 1-periodic extension of  $v_{\text{odd}}$ . We define the sequence  $\{z_n\}_{n \in \mathbb{Z}}$ :

$$z_n := v^*\left(\frac{n}{2^J}\right) \quad (n \in \mathbb{Z}). \quad (4.1)$$

So we obtain that for  $n \in \mathbb{Z}$  and  $l \in \mathbb{Z}$ ,

$$z_{-n} = -z_n, \quad z_{n+2^J} = z_n \quad \text{and} \quad z_{2^{J-1}l} = 0. \quad (4.2)$$

Hence  $\{z_n\}_{n \in \mathbb{Z}}$  can be determined by  $2^{J-1} - 1$  different values  $z_1, \dots, z_{2^{J-1}-1}$ .

## 4.2 The relationships between the coefficients in the HWT representation

Let  $\{c_{m,n}^{(1)}\}$  and  $\{d_{m,n}^{(1)}\}$  be periodic wavelet coefficients of  $v^* \in L^2\left([-\frac{1}{2}, \frac{1}{2}]\right)$ . Taking  $J$  sufficiently large, the following formula holds [1].

$$v^*(t) \simeq \sum_{n=0}^{2^J-1} c_{J,n}^{(1)} \tilde{\varphi}_{J,n}^{\text{per}}(t)$$

and

$$c_{J,n}^{(1)} \simeq v^*\left(\frac{n}{2^J}\right) = z_n. \quad (4.3)$$

By (2.4), we get

$$\sum_{k=0}^{2^J-1} c_{J,k}^{(1)} \tilde{\varphi}_{J,k}^{\text{per}} = \sum_{k=0}^{2^{J-1}-1} c_{J-1,k}^{(1)} \tilde{\varphi}_{J-1,k}^{\text{per}} + \sum_{k=0}^{2^{J-1}-1} d_{J-1,k}^{(1)} \tilde{\psi}_{J-1,k}^{\text{per}}.$$

By Proposition 2.1, we know that

$$c_{J-1,k}^{(1)} = \sum_{n=0}^{2^J-1} a_{n-2k}^* z_n \quad \text{and} \quad d_{J-1,k}^{(1)} = \sum_{n=0}^{2^J-1} b_{n-2k}^* z_n, \quad (4.4)$$

where  $\{a_n^*\}$  and  $\{b_n^*\}$  are stated in (2.7).

**Proposition 4.1.** Let  $c_{J-1,k}^{(1)} = \alpha_k$  ( $k = 1, \dots, 2^{J-2} - 1$ ) and  $d_{J-1,k}^{(1)} = \beta_k$  ( $k = 0, \dots, 2^{J-2} - 1$ ). Then

- (i)  $\left\{ c_{J-1,k}^{(1)} \right\}_{k=0}^{2^{J-1}-1} = \{0, \alpha_1, \dots, \alpha_{2^{J-2}-1}, 0, -\alpha_{2^{J-2}-1}, \dots, -\alpha_1\};$
- (ii)  $\left\{ d_{J-1,k}^{(1)} \right\}_{k=0}^{2^{J-1}-1} = \{\beta_0, \dots, \beta_{2^{J-2}-1}, -\beta_{2^{J-2}-1}, \dots, -\beta_0\}.$

We need a couple of lemmas.

**Lemma 4.2.** Let  $\{a_n^*\}$  and  $\{b_n^*\}$  be stated in (2.7). Then, for any  $n \in \mathbb{Z}$ ,

$$a_{-n}^* = a_n^* \quad \text{and} \quad b_n^* = b_{2-n}^*.$$

**Proof.** Since  $\varphi, \tilde{\varphi}$  are both real-valued even functions and  $a_n = \sqrt{2} \int_{\mathbb{R}} \varphi(t) \overline{\tilde{\varphi}(2t-n)} dt$  (by (2.5)), we have

$$\begin{aligned} a_{-n} &= \sqrt{2} \int_{\mathbb{R}} \varphi(t) \tilde{\varphi}(2t+n) dt \\ &= \sqrt{2} \int_{\mathbb{R}} \varphi(-t) \tilde{\varphi}(-2t+n) dt = \sqrt{2} \int_{\mathbb{R}} \varphi(t) \tilde{\varphi}(2t-n) dt = a_n. \end{aligned}$$

From this and (2.7), we get

$$a_{-n}^* = a_n^*, \quad a_{2^j+n}^* = a_n^* \quad (n \in \mathbb{Z}). \quad (4.5)$$

By (2.5),  $b_n = \sqrt{2} \int_{\mathbb{R}} \psi(t) \tilde{\varphi}(2t-n) dt$ . Since  $\psi(\frac{1}{2}-t) = \psi(\frac{1}{2}+t)$ , we have

$$\begin{aligned} b_n &= \sqrt{2} \int_{\mathbb{R}} \psi\left(\frac{1}{2}+t\right) \tilde{\varphi}(2t+1-n) dt = \sqrt{2} \int_{\mathbb{R}} \psi\left(\frac{1}{2}-t\right) \tilde{\varphi}(2t+1-n) dt \\ &= \sqrt{2} \int_{\mathbb{R}} \psi(t) \tilde{\varphi}(-2t+2-n) dt = \sqrt{2} \int_{\mathbb{R}} \psi(t) \tilde{\varphi}(2t-2+n) dt \\ &= b_{2-n}. \end{aligned}$$

So we get  $b_{1+n} = b_{1-n}$ . By (2.7), we have

$$b_{1+n}^* = b_{1-n}^* \quad (|n| \leq 2^{J-1}).$$

Again since  $b_{n+2^j}^* = b_n^*$ , we have  $b_{1+n}^* = b_{1-n}^*$  for all  $n \in \mathbb{Z}$ . So we get

$$b_n^* = b_{2-n}^* \quad (n \in \mathbb{Z}). \quad \square \quad (4.6)$$

**Lemma 4.3.** The periodic wavelet coefficients  $\{c_{m,n}^{(1)}\}$  and  $\{d_{m,n}^{(1)}\}$  satisfy the following relationships

$$c_{J-1,k}^{(1)} = -c_{J-1,2^{J-1}-k}^{(1)}, \quad d_{J-1,k}^{(1)} = -d_{J-1,2^{J-1}-k}^{(1)} \quad (k \in \mathbb{Z}). \quad (4.7)$$

**Proof.** From (4.2) and (4.5), it follows by (4.4) that

$$\begin{aligned} c_{J-1,2^{J-1}-k}^{(1)} &= \sum_{n=0}^{2^J-1} a_{n+2k-2^J}^* z_n \\ &= - \sum_{n=0}^{2^J-1} a_{n+2k}^* z_{-n} = - \sum_{n=-2^J+1}^0 a_{-n+2k}^* z_n \end{aligned}$$

Again thanks to the periodicity of the  $\{a_n\}$  and  $\{z_n\}$ , we have

$$\begin{aligned} \sum_{n=-2^J+1}^0 a_{-n+2k}^* z_n &= \sum_{n=1}^{2^J} a_{-n+2k}^* z_n = \sum_{n=1}^{2^J-1} a_{-n+2k}^* z_n + a_{2k-2^J}^* z_{2^J} \\ &= \sum_{n=1}^{2^J-1} a_{-n+2k}^* z_n + a_{2k} z_0 = \sum_{n=0}^{2^J-1} a_{-n+2k}^* z_n. \end{aligned} \quad (4.8)$$

So we have

$$c_{J-1,2^{J-1}-k}^{(1)} = - \sum_{n=0}^{2^J-1} a_{-n+2k}^* z_n = - \sum_{n=0}^{2^J-1} a_{n-2k}^* z_n = -c_{J-1,k}^{(1)}. \quad (4.9)$$

On the other hand, by (4.4) and (4.6),

$$\begin{aligned} d_{J-1,k}^{(1)} &= \sum_{n=0}^{2^J-1} b_{n-2k}^* z_n = \sum_{n=0}^{2^J-1} b_{2-n+2k}^* z_n \\ &= - \sum_{n=0}^{2^J-1} b_{2-n+2k}^* z_{-n} = - \sum_{n=-2^J+1}^0 b_{2+n+2k}^* z_n. \end{aligned} \quad (4.10)$$

By the similar argument to (4.8), we have

$$\sum_{n=-2^J+1}^0 b_{2+n+2k}^* z_n = \sum_{n=0}^{2^J-1} b_{2+n+2k}^* z_n.$$

So we get

$$d_{J-1,k}^{(1)} = - \sum_{n=0}^{2^J-1} b_{n-(2^J-2k-2)}^* z_n = -d_{J-1,2^{J-1}-k}^{(1)}. \quad \square$$

**Proof of Proposition 4.1.** By the first formula of (4.7), we get  $c_{J-1,2^{J-2}}^{(1)} = -c_{J-1,2^{J-2}}^{(1)}$ , i.e.,

$$c_{J-1,2^{J-2}}^{(1)} = 0. \quad (4.11)$$

Since  $a_n^* = a_{-n}^* = a_{2^J - n}^*$  and  $z_n = -z_{-n} = -z_{2^J - n}$ , by (4.4), we have

$$\begin{aligned} c_{J-1,0}^{(1)} &= \sum_{n=0}^{2^J-1} a_n^* z_n = \sum_{n=1}^{2^J} a_n^* z_n \\ &= - \sum_{n=1}^{2^J} a_{2^J-n}^* z_{2^J-n} = - \sum_{n=0}^{2^J-1} a_n^* z_n = -c_{J-1,0}^{(1)}. \end{aligned}$$

So  $c_{J-1,0}^{(1)} = 0$ .

Let  $c_{J-1,k}^{(1)} = \alpha_k$  ( $k = 0, \dots, 2^{J-1} - 1$ ). Then, by  $c_{J-1,0}^{(1)} = 0$ , and (4.9) and (4.11), we get

$$\alpha_0 = 0, \quad \alpha_{2^{J-2}} = 0, \quad \text{and} \quad \alpha_k = -\alpha_{2^{J-1}-k} \quad (k = 1, \dots, 2^{J-2} - 1).$$

i.e., (i) holds. Let  $d_{J-1,k}^{(1)} = \beta_k$  ( $k = 0, \dots, 2^{J-1} - 1$ ). By the second formula of (4.7), we have

$$\beta_k = -\beta_{2^{J-1}-1-k} \quad (k = 0, \dots, 2^{J-2} - 1),$$

i.e., (ii) holds. Proposition 4.1 is proved.  $\square$

From Proposition 4.1, we see that in order to recover the signal, we only need  $2^{J-1} - 1$  periodic wavelet coefficients and two boundary values of the signal  $f$ , the number of the sampling points  $\{x_n\}_0^{2^J-1}$  is just  $2^{J-1} + 1$ .

So the 1D HWT is not a redundant transform.

### 4.3 Two-dimensional discrete HWT

We will now discuss two-dimensional discrete HWT and study the symmetry property of the coefficients.

Let an image  $f \in C^2 \left( \left[0, \frac{1}{2}\right]^2 \right)$ . For some large  $J$ , take the  $(2^{J-1} + 1)^2$  sample points of  $f$

$$x_{n_1, n_2} = f \left( \frac{n_1}{2^J}, \frac{n_2}{2^J} \right) \quad (n_1, n_2 = 0, \dots, 2^{J-1}).$$

Using the HWT decomposition, we get

$$f(x, y) = u(x, y) + v(x, y) \quad \left( (x, y) \in \left[0, \frac{1}{2}\right]^2 \right),$$

where  $u(x, y)$  is a harmonic function satisfying Laplace's equation  $\Delta u = 0$  and  $u = f$  on the boundary of  $\left[0, \frac{1}{2}\right]^2$ .

We can efficiently and accurately compute  $u$  by using the Averbuch-Israeli-Vozovoi (AIV) method [2]. Let us now discuss the residual component  $v$ .

Let  $y_{n_1, n_2} = v\left(\frac{n_1}{2^J}, \frac{n_2}{2^J}\right)$ . Then

$$y_{0, n_2} = y_{n_1, 0} = y_{2^{J-1}, n_2} = y_{n_1, 2^{J-1}} = 0 \quad (n_1, n_2 = 0, \dots, 2^{J-1}).$$

Let  $v_{\text{odd}}$  be an odd extension of  $v$  to  $[-\frac{1}{2}, \frac{1}{2}]^2$ , i.e.,

$$v_{\text{odd}}(x, y) = v(x, y) \quad \left( (x, y) \in \left[0, \frac{1}{2}\right]^2 \right)$$

and

$$v_{\text{odd}}(x, y) = -v_{\text{odd}}(-x, y) = -v_{\text{odd}}(x, -y) = v_{\text{odd}}(-x, -y), \quad \left( (x, y) \in \left[-\frac{1}{2}, \frac{1}{2}\right]^2 \right).$$

Denote  $z_{n_1, n_2} = v_{\text{odd}}\left(\frac{n_1}{2^J}, \frac{n_2}{2^J}\right)$ . Then

$$z_{n_1, n_2} = -z_{-n_1, n_2} = -z_{n_1, -n_2} = z_{-n_1, -n_2} \quad (n_1, n_2 = 0, \pm 1, \dots, \pm 2^{J-1}) \quad (4.12)$$

and

$$z_{0, n_2} = z_{n_1, 0} = z_{2^{J-1}, n_2} = z_{n_1, 2^{J-1}} = z_{-2^{J-1}, n_2} = z_{n_1, -2^{J-1}} = 0.$$

Let  $v^*$  be a 1-periodic extension of  $v_{\text{odd}}$  to  $\mathbb{R}^2$ . Denote  $z_{n_1, n_2}^* = v^*\left(\frac{n_1}{2^J}, \frac{n_2}{2^J}\right)$ . Then

$$z_{n_1, n_2}^* = z_{n_1, n_2}, \quad (n_1, n_2 = 0, \pm 1, \dots, \pm 2^{J-1}),$$

$$z_{n_1+2^J, n_2}^* = z_{n_1, n_2}^*, \quad z_{n_1, n_2+2^J}^* = z_{n_1, n_2}^*, \quad (n_1 \in \mathbb{Z}, n_2 \in \mathbb{Z}). \quad (4.13)$$

For  $\mu = 1, 2, 3$ ,  $m \in \mathbb{Z}$ ,  $n \in \mathbb{Z}^2$ , let  $c_{m, n_1, n_2}^{(2)}$  and  $d_{\mu, m, n_1, n_2}^{(2)}$  be the periodic wavelet coefficients of  $v^* \in L^2\left(\left[-\frac{1}{2}, \frac{1}{2}\right]^2\right)$  (see (2.9)).

Take  $J$  sufficiently large such that

$$v^*(x, y) \simeq \sum_{n_1, n_2=0}^{2^J-1} c_{J, n}^{(2)} \tilde{\varphi}_{0, J, n}^{\text{per}} \quad \text{and} \quad c_{J, n}^{(2)} \simeq v^*\left(\frac{n_1}{2^J}, \frac{n_2}{2^J}\right) = z_{n_1, n_2}^*, \quad n = (n_1, n_2).$$

Again, by (2.11), we have

$$v^*(x, y) \simeq \sum_{n_1, n_2=0}^{2^{J-1}-1} c_{J-1, n_1, n_2}^{(2)} \tilde{\varphi}_{0, J-1, n_1, n_2}^{\text{per}} + \sum_{\mu=1}^3 \sum_{n_1, n_2=0}^{2^{J-1}-1} d_{\mu, J-1, n_1, n_2}^{(2)} \tilde{\psi}_{\mu, J-1, n_1, n_2}^{\text{per}}. \quad (4.14)$$

Now we discuss the symmetry property of the coefficients  $c_{J-1, k_1, k_2}^{(2)}$  and  $d_{\mu, J-1, k_1, k_2}^{(2)}$ . From Proposition 2.2, Lemma 4.2, (4.12), and (4.13), we can get

**Proposition 4.4.** For  $k_1, k_2 \in \mathbb{Z}$ , we have

$$(i) \quad c_{J-1, 2^{J-1}-k_1, k_2}^{(2)} = -c_{J-1, k_1, k_2}^{(2)}, \quad c_{J-1, k_1, 2^{J-1}-k_2}^{(2)} = -c_{J-1, k_1, k_2}^{(2)}, \quad c_{J-1, 2^{J-2}, k_2}^{(2)} = c_{J-1, 0, k_2}^{(2)} = c_{J-1, k_1, 2^{J-2}}^{(2)} = c_{J-1, k_1, 0}^{(2)} = 0;$$

$$(ii) \quad d_{1, J-1, 2^{J-1}-k_1, k_2}^{(2)} = -d_{1, J-1, k_1, k_2}^{(2)}, \quad d_{1, J-1, k_1, 2^{J-1}-k_2-1}^{(2)} = -d_{1, J-1, k_1, k_2}^{(2)}, \quad d_{1, J-1, 2^{J-2}, k_2}^{(2)} = d_{1, J-1, 0, k_2}^{(2)} = 0;$$

$$(iii) \quad d_{2, J-1, 2^{J-1}-k_1-1, k_2}^{(2)} = -d_{2, J-1, k_1, k_2}^{(2)}, \quad d_{2, J-1, k_1, 2^{J-1}-k_2}^{(2)} = -d_{2, J-1, k_1, k_2}^{(2)}, \quad d_{2, J-1, k_1, 2^{J-2}}^{(2)} = d_{2, J-1, k_1, 0}^{(2)} = 0; \text{ and}$$

$$(iv) \quad d_{3, J-1, 2^{J-1}-k_1-1, k_2}^{(2)} = -d_{3, J-1, k_1, k_2}^{(2)}, \quad d_{3, J-1, k_1, 2^{J-1}-k_2-1}^{(2)} = -d_{3, J-1, k_1, k_2}^{(2)}.$$

From Proposition 4.4, the symmetry of the matrix  $(c_{J-1, k_1, k_2}^{(2)})$ ,  $k_1, k_2 = 0, 1, \dots, 2^{J-1} - 1$  is described as follows:

$$\begin{pmatrix} 0 & 0 & \cdots & 0 & 0 & 0 & \cdots & 0 \\ 0 & \alpha_{1,1} & \cdots & \alpha_{1,2^{J-2}-1} & 0 & -\alpha_{1,2^{J-2}-1} & \cdots & -\alpha_{1,1} \\ \vdots & \vdots \\ 0 & \alpha_{2^{J-2}-1,1} & \cdots & \alpha_{2^{J-2}-1,2^{J-2}-1} & 0 & -\alpha_{2^{J-2}-1,2^{J-2}-1} & \cdots & -\alpha_{2^{J-2}-1,1} \\ 0 & 0 & \cdots & 0 & 0 & 0 & \cdots & 0 \\ 0 & -\alpha_{2^{J-2}-1,1} & \cdots & -\alpha_{2^{J-2}-1,2^{J-2}-1} & 0 & \alpha_{2^{J-2}-1,2^{J-2}-1} & \cdots & \alpha_{2^{J-2}-1,1} \\ \vdots & \vdots \\ 0 & -\alpha_{1,1} & \cdots & -\alpha_{1,2^{J-2}-1} & 0 & \alpha_{2^{J-2}-1,2^{J-2}-1} & \cdots & \alpha_{2^{J-2}-1,1} \end{pmatrix}$$

where

$$\alpha_{k_1, k_2} = c_{J-1, k_1, k_2}^{(2)} \quad (k_1, k_2 = 1, \dots, 2^{J-2} - 1),$$

Therefore, the matrix  $\left(c_{J-1,k_1,k_2}^{(2)}\right)$ ,  $k_1, k_2 = 0, 1, \dots, 2^{J-1} - 1$ , is determined by  $(2^{J-2} - 1)^2$  values. Similarly, we have

- (i) the matrix  $\left(d_{1,J-1,k_1,k_2}^{(2)}\right)$ ,  $k_1, k_2 = 0, \dots, 2^{J-1} - 1$ , is determined by  $2^{J-2} (2^{J-2} - 1)$  values;
- (ii) the matrix  $\left(d_{2,J-1,k_1,k_2}^{(2)}\right)$ ,  $k_1, k_2 = 0, \dots, 2^{J-1} - 1$ , is determined by  $2^{J-2} (2^{J-2} - 1)$  values; and
- (iii) the matrix  $\left(d_{3,J-1,k_1,k_2}^{(2)}\right)$ ,  $k_1, k_2 = 0, \dots, 2^{J-1} - 1$ , is determined by  $2^{2J-4}$  values.

Noticing that

$$(2^{J-2} - 1)^2 + 2^{J-2} (2^{J-2} - 1) + 2^{J-2} (2^{J-2} - 1) + 2^{2J-4} = (2^{J-1} - 1)^2.$$

we know that in order to recover  $v^*$ , we only need  $(2^{J-1} - 1)^2$  periodic wavelet coefficients. To obtain the harmonic function  $u$ , we need  $4(2^{J-1} - 1) + 4$  boundary sample points of the image  $f$  on  $\partial\left([0, \frac{1}{2}]^2\right)$ . Since the number

$$(2^{J-1} - 1)^2 + 4(2^{J-1} - 1) + 4 = (2^{J-1} + 1)^2$$

is exactly equal to the number of sampling points of  $f$ , i.e., *the 2D HWT is not redundant*.

## 5 Image Approximation Experiments via HWT

We will examine the approximation performance of the 2D HWT algorithm. The quality of approximation in this paper is measured by PSNR (or peak signal-to-noise ratio) defined as

$$\text{PSNR} := 20 \times \log_{10} \left( \max_{x \in \bar{\Omega}} |f(x)| / \text{RMSE} \right),$$

where RMSE is the absolute  $\ell^2$  error between the original and the approximation divided by the square root of the total number of pixels in the original image. The unit of PSNR is decibel (dB).

### 5.1 Comparison with the periodic and folded wavelet algorithms

To approximate an image sampled on a square by the 2D HWT algorithm, we first decompose the image into the harmonic component  $u$  and the residual  $v$  (see Fig. 1). The harmonic component  $u$  is determined by the

data at boundary of the square. Hence in order to approximate  $u$ , it suffices to approximate the data on the boundary of the square. Since the boundary consists of four segments, we simply apply one-dimensional LLST on each segment. For the residual  $v$ , we do an odd extension and a periodic extension (see Fig. 2) and expand it into a periodic wavelet series with respect to a biorthonormal periodic wavelet basis with the symmetric filter bank (see Fig. 3). Our image approximation and reconstruction strategy consists of the following steps: 1) Retain the gray values of the four corner pixels of the image that are necessary to compute the 1D harmonic component of each boundary segment of the square; 2) Select a certain number of the largest coefficients in terms of energy from the rest of the coefficients (both 1D and 2D); 3) Reconstruct  $u$  and  $v$  from these retained coefficients using the AIV algorithm [2] and the Mallat algorithm, respectively; and 4) Compute  $u + v$ .

For approximation and reconstruction of the image by the periodic wavelet algorithm and the folded wavelet algorithm, we simply retain a certain number of the largest coefficients in terms of energy from all the coefficients and reconstruct the image from them.

First, we compare the performance of HWT with that of the periodic wavelet transform (PWT) and the folded wavelet transform (FWT). We use the 9/7 biorthogonal filter bank (see [7, Sec. 7.4] for the actual filter coefficients). The depths of decomposition  $J$  we test here are  $J = 2, 4, \log_2(N)$  for an image of size  $N \times N$ . The original image sizes we use are all dyadic, i.e.,  $N = 2^n$ , which are suitable for PWT and FWT. Hence, for HWT, we duplicate the last column and row of each image to make it suitable for HWT.

As for the images, we use the face part of Barbara image (with  $128 \times 128$  pixels) as well as the standard images “Bridge”, “Truck”, and “Moon surface”, each of which consists of  $256 \times 256$  pixels. Fig. 4 shows the latter three images.

Fig. 5, 6, and 7 show the quality of approximations of these four images when the depth of decomposition  $J$  is set to two, four, and maximum (seven for the Barbara face image and eight for the other three images), respectively. From these figures, the performance of HWT is consistently superior to that of PWT and FWT. For  $J = 2$ , we observe that the big performance difference between HWT and that of PWT and FWT particularly

when the ratio of the retained coefficients is less than about 6%. This can be explained as follows. For any image of size  $N \times N$ , if the depth of decomposition  $J$  is set to 2, then the number of low-pass wavelet coefficients in PWT and FWT is  $N^2/16$ , i.e., very large. Since the low-pass wavelet coefficients are not sparse, we need many coefficients to approximate such an image well. In other words, we cannot efficiently approximate such an image using a small number of coefficients if  $J$  is set to a small number such as 2. In fact,  $N^2/16$  is 6.25% of the original image size  $N^2$ , which agrees with our observation. On the other hand, HWT decomposes an image into two components: the harmonic component and the residual. We can approximate the harmonic component very well using a few 1D LLST coefficients. For the residual, we still have the same problem as PWT and FWT if  $J = 2$ . However, since the norm of the residual is much smaller than that of the original image thanks to the removal of the harmonic component, the reconstruction error is kept small.

When  $J = 4$  or  $J$  is set to its maximum, the performance of HWT is about 0.2 ~ 0.5dB better than that of PWT, and the 0.1 ~ 0.2dB better than that of FWT. In general, the smaller the number of the retained coefficients, the clearer the performance difference becomes. This is also due to the harmonic component in HWT.

We now would like to show the reconstructed images because the PSNR plots do not tell the whole story. Fig. 8, 9, and 10 show the reconstructed Barbara face images using top 5% coefficients of PWT, FWT, and HWT for  $J = 2, 4, 7$ , respectively. From these figures, we can see that the HWT algorithm is also *perceptually* better than the PWT algorithm and the FWT algorithm, particularly for  $J = 2$ . We can also notice some difference around the frame boundary of the images. This is due to the use of LLST on the boundary pixels in HWT. Overall, for each algorithm, the difference between  $J = 4$  and  $J = 7$  is not noticeable.

## 5.2 Comparison with LLST

We now compare the HWT algorithm with the LLST algorithm. In general, the decay rate of LLST coefficients depends on global smoothness of the input data while that of HWT coefficients depends on local smoothness. Since the global smoothness of a function is determined by its rough part (even if that part is localized), we

need fewer HWT coefficients than LLST coefficients in order to reconstruct the data to the same quality. For LLST, we divide the image into several blocks and do LLST on each block. The size of block we use in our experiments is  $9 \times 9$ ,  $17 \times 17$ ,  $33 \times 33$ ,  $65 \times 65$ ,  $129 \times 129$  for all the four images, and in addition, we use  $257 \times 257$  block for the “Bridge”, “Truck”, and “Moon Surface” images. Note that the largest block size for each image implies that LLST does not divide it into a set of smaller segments. We first retain all the corner pixel values of each block, select the certain number of coefficients with the largest energy among all the coefficients (both 1D and 2D) not yet used, reconstruct an approximation from these coefficients, and finally evaluate its quality of approximation. For HWT, the depth of decomposition is set to the maximum, and we also use the 9/7 biorthonormal filter bank. We apply HWT on the whole image and retain the coefficients with the largest energy. Fig. 11 shows the quality of approximation by PSNR values when we retain 2%-20% of the original coefficients. From this figure, we again observe that HWT consistently outperforms LLST regardless of the block sizes. In particular, HWT’s performance is significantly better (about 1dB) than that of LLST for the “Bridge”, “Truck”, and “Moon Surface” images while its performance on “Barbara face” image is closely followed by that of LLST with  $17 \times 17$  blocks, especially around the ratio of the number of the retained coefficients to that of the original coefficients ranges around 8% to 10%. We believe that this is due to the existence of textures in the Barbara face image. We also observe that the performance of LLST at a particular ratio of the number of the retained coefficients to that of the whole coefficient strongly depends on the block size. For example, for heavy compression (i.e., the ratio is about 2% to 8%), the LLST with the larger block sizes perform better than that with the smaller block sizes while the situation is opposite if one can afford to keep a larger number of coefficients (e.g., the ratio is larger than 10%). HWT does not require the user to choose any such block sizes, which is one of the major advantage of HWT over LLST.

### 5.3 Comparison with wavelets on the interval

It is appropriate to compare HWT with wavelets on the interval (WOI) introduced by Cohen, Daubechies and Vial [5] because WOI also tries to overcome boundary effects. Compared to HWT, the periodic wavelets, and

folded wavelets, however, the construction of WOI is quite complicated. Their starting point is Daubechies’s compactly supported scaling functions and wavelets. They first construct scaling functions on the interval consisting of three parts: the left edge scaling function, the interior scaling function, and the right edge scaling function. Then, they use these scaling functions on the interval to construct the corresponding wavelets also consisting of three parts: the left edge wavelet, the interior wavelet, and the right edge wavelet. Although these wavelets on the interval have high vanishing moments, we cannot apply its discrete version to image approximation immediately. This is because their corresponding high pass filter cannot map a simple polynomial sequence to zero. So when one uses WOI to approximate images, one has to perform a prefiltering (or preconditioning) on the data first; see [5] for the detail.

We now compare the performance of HWT with that of WOI. Since the harmonic component of HWT takes care of linear parts on the boundary, in order to be a fair comparison with HWT, we use WOI with two vanishing moments. For HWT, we use Villasenor 5/3 filter bank [10], which also has two vanishing moments. Fig. 12 shows the quality of approximation measured by PSNR values when we retain 1% – 10% of the original coefficients. The depth of decomposition for both HWT and WOI is set to five for the Barbara face image and six for the other three images since these are the maximal depth of decomposition that the WOI can take. From this figure, we observe that that HWT again consistently outperforms WOI. Considering the implementation complexity of WOI, HWT should be used if one wants to reduce the boundary effects.

## 6 Conclusion

In this paper, we proposed the Harmonic Wavelet Transform (HWT) that is not affected by the boundary of input data. The idea of removing the boundary mismatches of input data originally proposed in LLST [8] is quite important since the residual component after odd reflection and periodization, say, the  $v^*$  component, does not contain any artificial discontinuities caused by the boundary mismatches. Hence, the expansion coefficients of  $v^*$  with respect to the periodic wavelet basis truly reflect the local smoothness of an input image. Moreover,

HWT captures the intrinsic singularities in the interior of the domain more efficiently than LLST that uses the Fourier sine series expansion for  $v^*$ . Also, the implementation of HWT is simpler than WOI because HWT does not need any special boundary-dependent filter banks. Finally, our image approximation experiments using four standard images demonstrated the superiority of HWT over LLST, PWT, FWT, and WOI. We also note that the extension of HWT to a higher dimension is straightforward thanks to the efficient Laplace solver for higher dimension [3].

## Acknowledgment

This research was partially supported by the NSF grant DMS-0410406, the ONR grants N00014-07-1-0166, N00014-09-1-0041, and N00014-09-1-0318. For computing the periodic and folded wavelet transforms as well as the wavelets on interval, we used the WaveLab software developed by Prof. David Donoho of Stanford Univ. and his team [6].

## References

- [1] M. Antonini, M. Barlaud, P. Mathieu, and I. Daubechies, Image coding using wavelet transform, *IEEE Trans. Image Proc.* 1 (2) (1992) 205–220.
- [2] A. Averbuch, M. Israeli, and L. Vozovoi, A fast Poisson solver of arbitrary order accuracy in rectangular regions, *SIAM J. Sci. Comput.* 19 (1998) 933–952.
- [3] E. Braverman, M. Israeli, A. Averbuch, L. Vozovoi, A fast 3D Poisson solver of arbitrary order accuracy, *J. Comput. Phys.* 144 (1998) 109–136.
- [4] C. K. Chui, *An Introduction to Wavelets*, Academic Press, San Diego, 1992.
- [5] A. Cohen, I. Daubechies, and P. Vial, Wavelet bases on the interval and fast algorithms, *Appl. Comput. Harmon. Anal.* 1 (1993) 54–81.

- [6] D. Donoho *et al.*, <http://www-stat.stanford.edu/~wavelab>.
- [7] S. Mallat, *A Wavelet Tour of Signal Processing* (Third edition), Academic Press, San Diego, 2009.
- [8] N. Saito and J. Remy, The polyharmonic local sine transform: a new tool for local image analysis and synthesis without edge effect, *Appl. Comp. Harmon. Anal.* 31 (2006) 41–73.
- [9] D. Van De Ville, T. Blu, and M. Unser, Isotropic polyharmonic B-splines: Scaling functions and wavelets, *IEEE Trans. Image Proc.* 14 (11) (2005) 1798–1813.
- [10] J. D. Villasenor, B. Belzer, and J. Liao, Wavelet filter evaluation for image compression, *IEEE Trans. Image Proc.* 4 (8) (1995) 1053–1060.

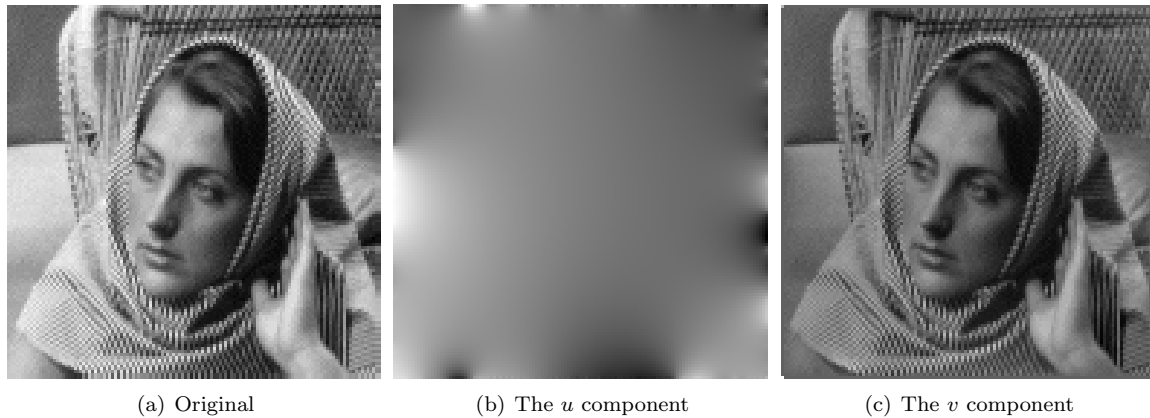


Figure 1: HWT decomposition of the Barbara face image. Each image is displayed using its full dynamic range.



Figure 2: The odd extension of the residual component  $v$ .

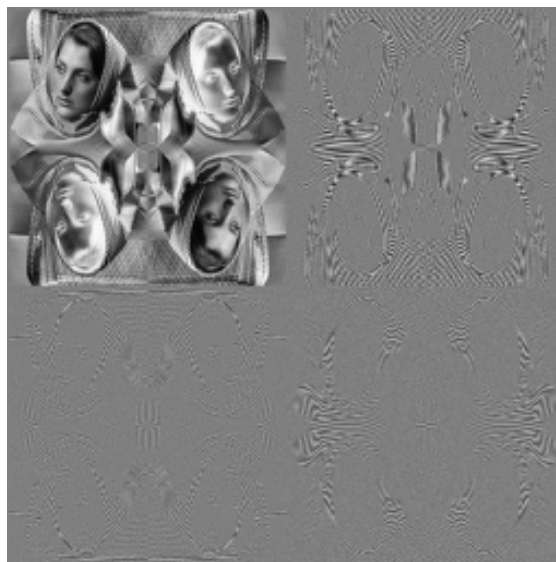


Figure 3: The periodic biorthonormal wavelet coefficients of the odd extension of the residual component  $v$  when the depth of decomposition is one.

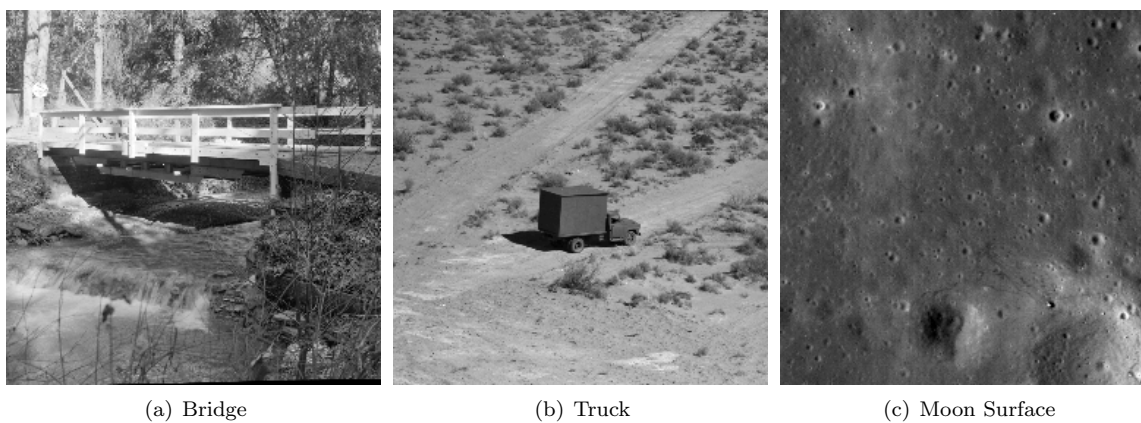


Figure 4: The three more standard images used in our experiments.

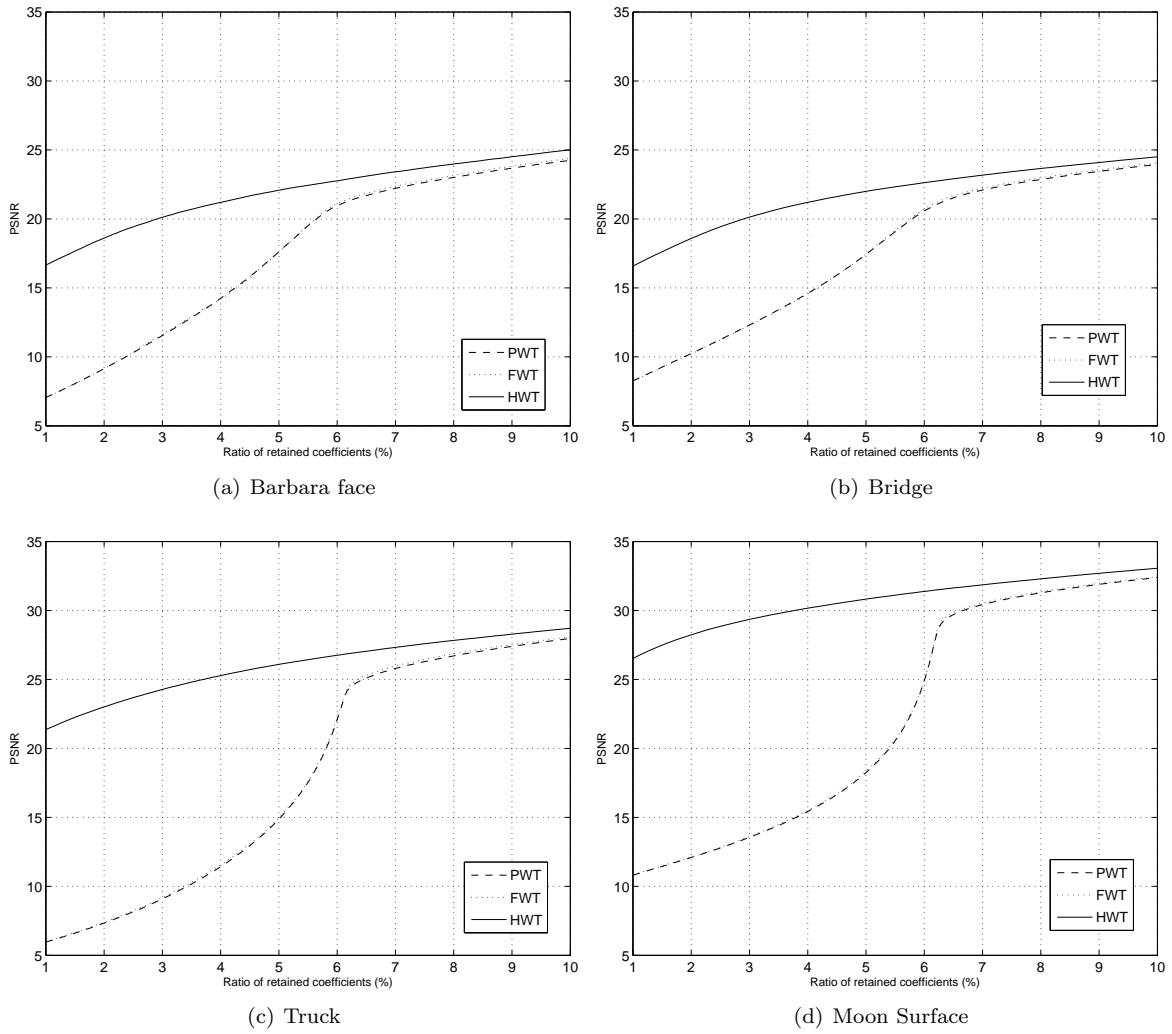
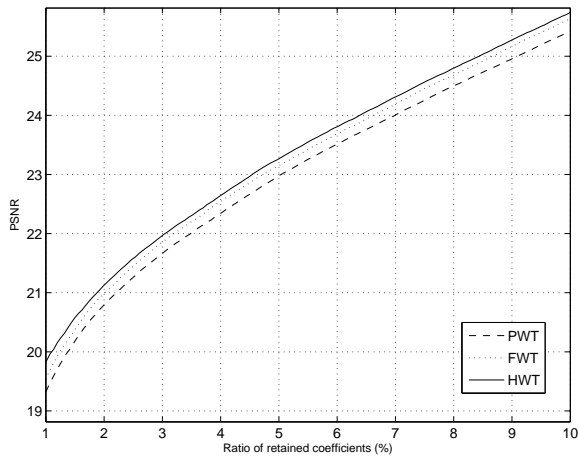
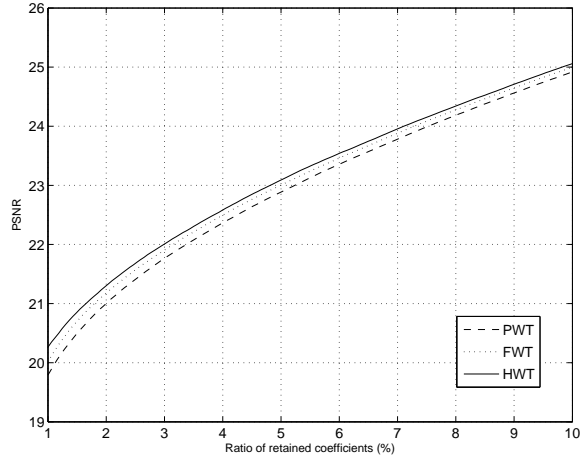


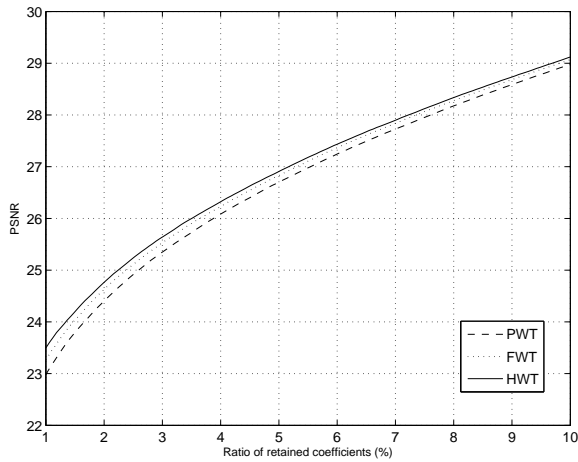
Figure 5: Quality of approximation of the four standard images measured by PSNR values as a function of the ratio of the number of the retained coefficients to the total number of the coefficients. The depth of decomposition is set to two in each case.



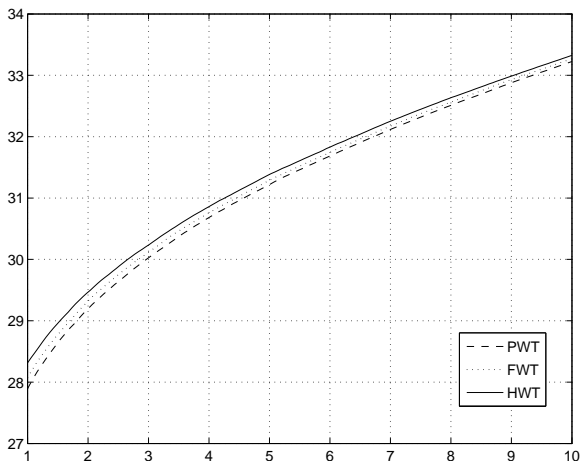
(a) Barbara face



(b) Bridge



(c) Truck



(d) Moon Surface

Figure 6: Quality of approximation of the four standard images measured by PSNR values as a function of the ratio of the number of the retained coefficients to the total number of the coefficients. The depth of decomposition is set to four in each case.

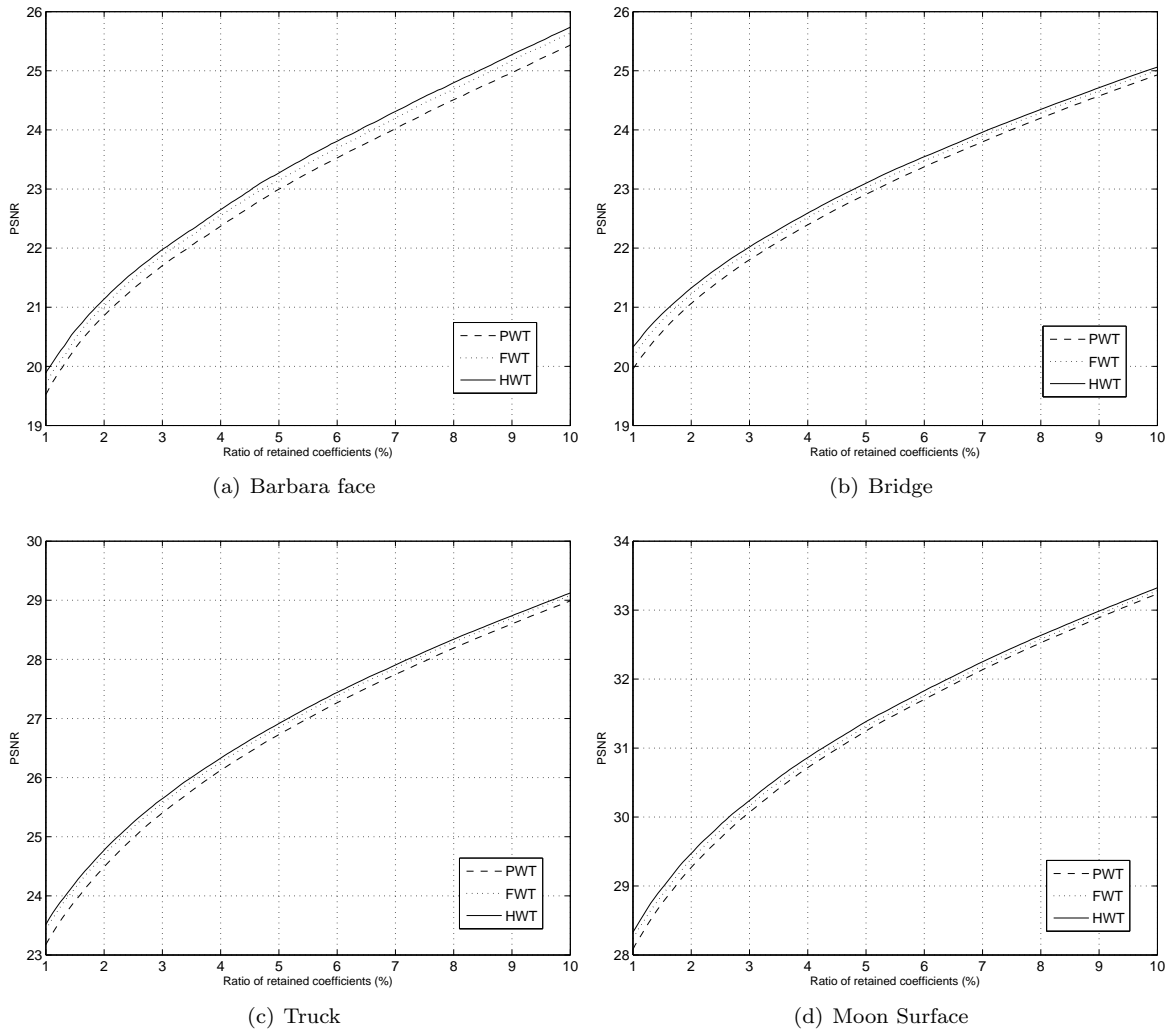


Figure 7: Quality of approximation of the four standard images measured by PSNR values as a function of the ratio of the number of the retained coefficients to the total number of the coefficients. The depth of decomposition is set to the maximum in each case, i.e., seven for the Barbara face image and eight for the others.



(a) Original Image



(b) PWT



(c) FWT



(d) HWT

Figure 8: Approximations of the Barbara face image using the top 5% coefficients when the depth of decomposition is two. The PSNR values (in dB) of PWT, FWT, and HWT are 17.6182, 17.5961, and 22.0776, respectively.



(a) Original Image



(b) PWT



(c) FWT



(d) HWT

Figure 9: Approximations of the Barbara face image using the top 5% coefficients when the depth of decomposition is four. The PSNR values (in dB) of PWT, FWT, and HWT are 22.9791, 23.1484, and 23.2651, respectively.



(a) Original Image



(b) PWT



(c) FWT



(d) HWT

Figure 10: Approximations of the Barbara face image using the top 5% coefficients when the depth of decomposition is seven. The PSNR values (in dB) of PWT, FWT, and HWT are 22.9962, 23.1476, and 23.2688, respectively.

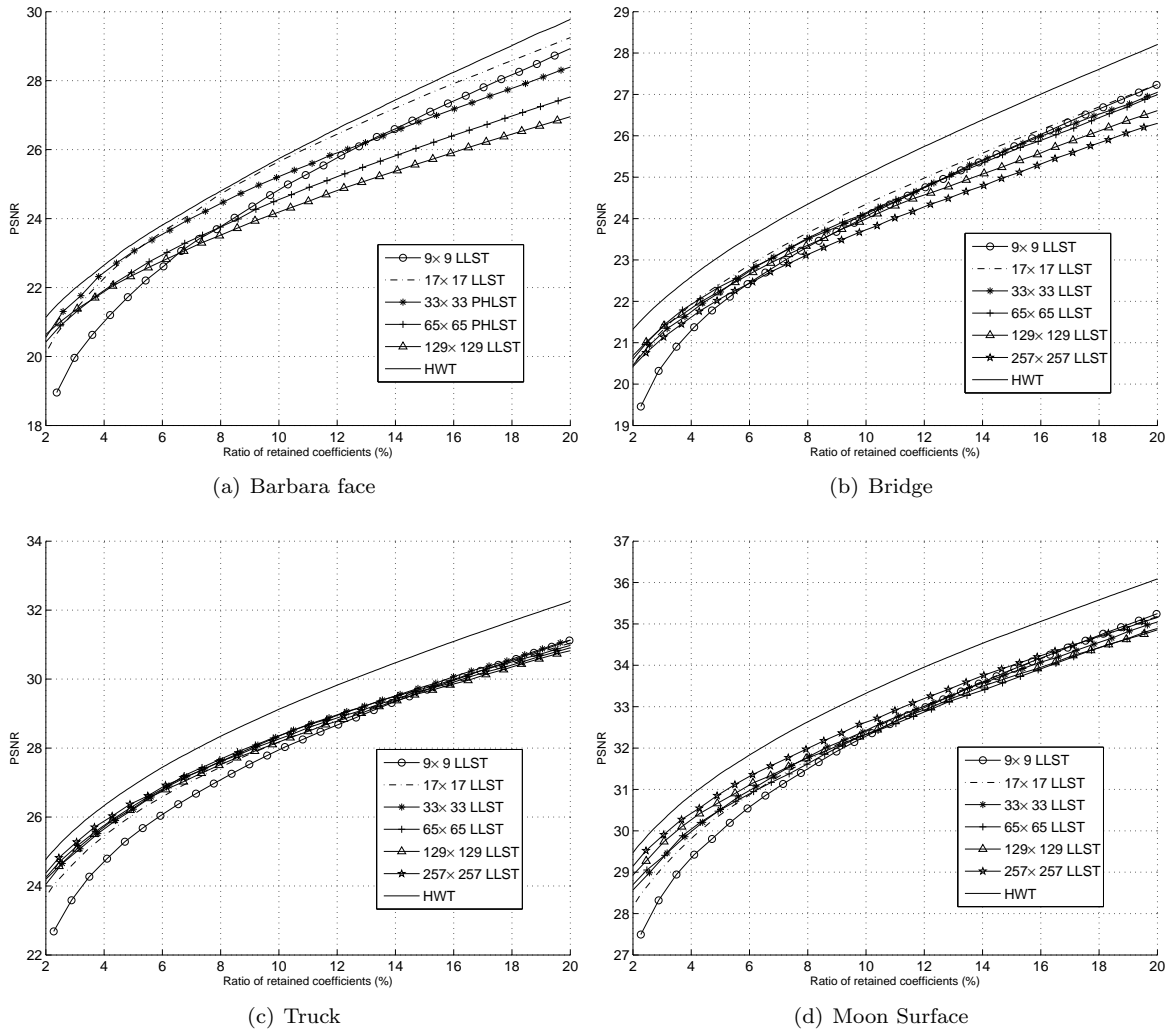


Figure 11: Quality of approximation of the four standard images measured by PSNR values as a function of the ratio of the number of the retained coefficients to the total number of the coefficients. These figures compare the performance of HWT with that of LLST with different block sizes. For HWT, the depth of decomposition is set to its maximum level.

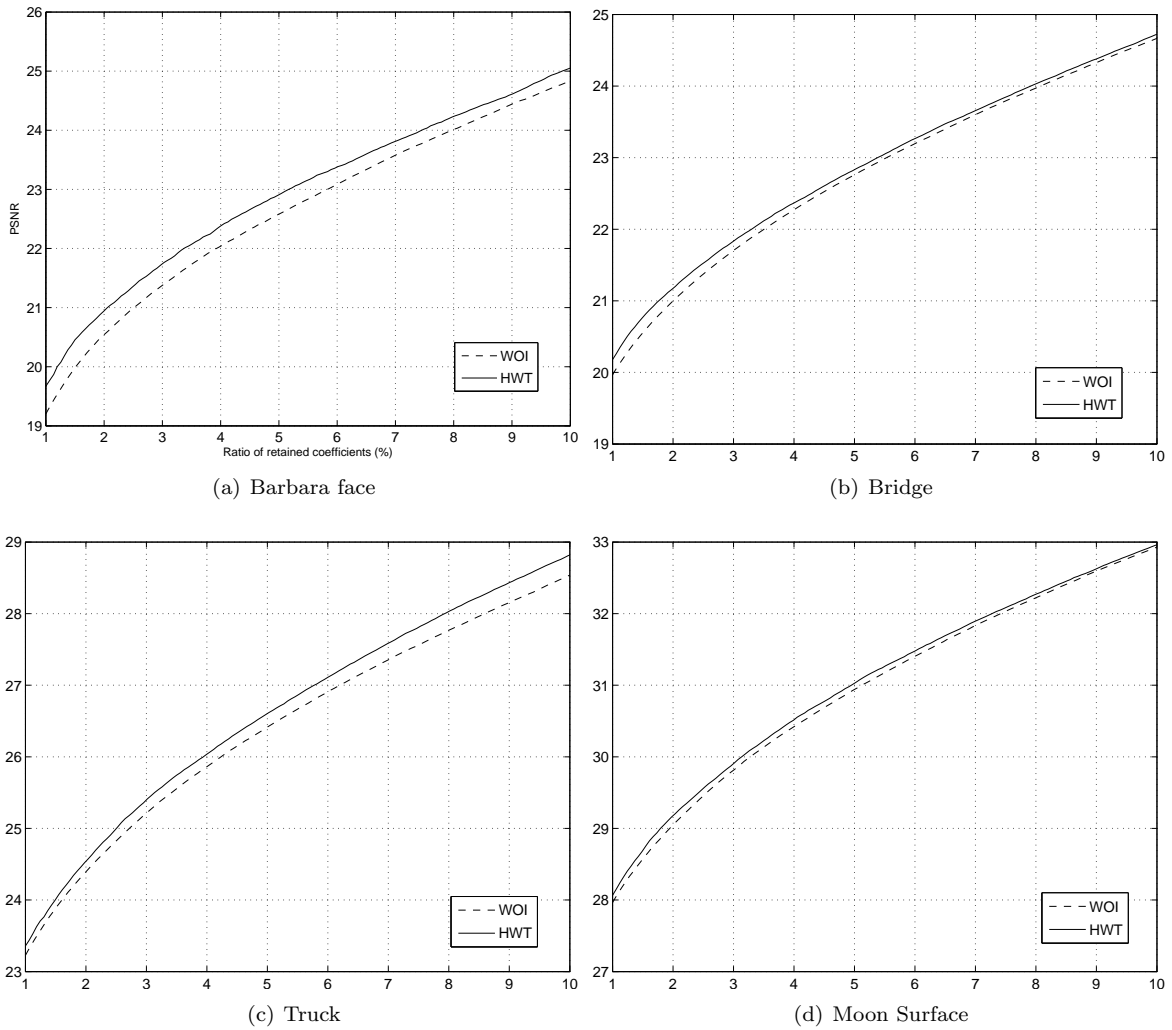


Figure 12: Quality of approximation of the four standard images measured by PSNR values as a function of the ratio of the number of the retained coefficients to the total number of the coefficients. These figures compare the performance of HWT with that of WOI. For both HWT and WOI, the depth of decomposition is set to its maximum possible level.